Acta Oceanol. Sin., 2017, Vol. 36, No. 12, P. 1–10
DOI: 10.1007/s13131-017-1098-8
http://www.hyxb.org.cn
E-mail: hyxbe@263.net

Comparison of air-sea CO_2 flux and biological productivity in the South China Sea, East China Sea, and Yellow Sea: a three-dimensional physical-biogeochemical modeling study

JI Xuanliang[1, 2], LIU Guimei[1, 2*], GAO Shan[1, 2], WANG Hui[1, 2], ZHANG Miaoyin[1, 2]

[1] National Marine Environmental Forecasting Center, Beijing 100081, China

[2] Key Laboratory of Research on Marine Hazards Forecasting, National Marine Environmental Forecasting Center, State Oceanic Administration, Beijing 100081, China

Received 1 March 2017; accepted 16 June 2017

Abstract

Marginal seas play important roles in regulating the global carbon budget, but there are great uncertainties in estimating carbon sources and sinks in the continental margins. A Pacific basin-wide physical-biogeochemical model is used to estimate primary productivity and air-sea CO_2 flux in the South China Sea (SCS), the East China Sea (ECS), and the Yellow Sea (YS). The model is forced with daily air-sea fluxes which are derived from the NCEP2 reanalysis from 1982 to 2005. During the period of time, the modeled monthly-mean air-sea CO_2 fluxes in these three marginal seas altered from an atmospheric carbon sink in winter to a source in summer. On annual-mean basis, the SCS acts as a source of carbon to the atmosphere (16 Tg/a, calculated by carbon, released to the atmosphere), and the ECS and the YS are sinks for atmospheric carbon (–6.73 Tg/a and –5.23 Tg/a, respectively, absorbed by the ocean). The model results suggest that the sea surface temperature (SST) controls the spatial and temporal variations of the oceanic pCO_2 in the SCS and ECS, and biological removal of carbon plays a compensating role in modulating the variability of the oceanic pCO_2 and determining its strength in each sea, especially in the ECS and the SCS. However, the biological activity is the dominating factor for controlling the oceanic pCO_2 in the YS. The modeled depth-integrated primary production (IPP) over the euphotic zone shows seasonal variation features with annual-mean values of 293, 297, and 315 mg/(m^2·d) in the SCS, the ECS, and the YS, respectively. The model-integrated annual-mean new production (uptake of nitrate) values, as in carbon units, are 103, 109, and 139 mg/(m^2·d), which yield the *f*-ratios of 0.35, 0.37, and 0.45 for the SCS, the ECS, and the YS, respectively. Compared to the productivity in the ECS and the YS, the seasonal variation of biological productivity in the SCS is rather weak. The atmospheric pCO_2 increases from 1982 to 2005, which is consistent with the anthropogenic CO_2 input to the atmosphere. The oceanic pCO_2 increases in responses to the atmospheric pCO_2 that drives air-sea CO_2 flux in the model. The modeled increase rate of oceanic pCO_2 is 0.91 μatm/a in the YS, 1.04 μatm/a in the ECS, and 1.66 μatm/a in the SCS, respectively.

Key words: physical-biogeochemical model, air to sea CO_2 flux, South China Sea, East China Sea, Yellow Sea

Citation: Ji Xuanliang, Liu Guimei, Gao Shan, Wang Hui, Zhang Miaoyin. 2017. Comparison of air-sea CO_2 flux and biological productivity in the South China Sea, East China Sea, and Yellow Sea: a three-dimensional physical-biogeochemical modeling study. Acta Oceanologica Sinica, 36(12): 1–10, doi: 10.1007/s13131-017-1098-8

1 Introduction

The ocean is the largest active carbon reservoir on Earth. On time scales ranging from sub-diurnal to decadal, ocean carbon shows significant spatial and temporal variation characteristics (Takahashi et al., 2002). Globally, the ocean uptake of anthropogenic CO_2 is estimated about 2 Pg/a (calculated by carbon) (Fletcher et al., 2006; Takahashi et al., 2009), about one-third of total anthropogenic CO_2 emitted. These global estimations, however, have not fully accounted for carbon fluxes in the continental margins, which have potential importance in absorbing anthropogenic CO_2 (Walsh, 1991). Recently, the role of continental margins in the global carbon budget has aroused great research interest (Chen et al., 2004; Cai et al., 2006). Since the China's seas, including the South China Sea (SCS), the East China Sea (ECS), the Yellow Sea (YS), and the Bohai Sea, are the largest continental marginal seas in the western Pacific Ocean, studying these seas is therefore very important for quantifying the role of marginal seas in the global carbon cycle.

The YS, located between China and Korea, has a maximum depth of 103 m and an average water depth of 44 m (Fig. 1). The deepest part of the YS is in the central area with a trough, called the Yellow Sea Trough. The ECS has a broad continental shelf break, bounded by the Ryukyu Island chain. It opens at the north to the YS, and is connected with the Sea of Japan by the Tsushima Strait and with the SCS by the Taiwan Strait in the south. The SCS, with an abyssal basin more than 3 000 m deep, is separated

Foundation item: The National Key Research and Development Program of China under contract No. 2016YFC1401605; the Strategic Priority Research Program of the Chinese Academy of Sciences under contract No. XDA 1102010403; the National Natural Science Foundation of China under contract Nos 41222038, 41206023 and 41406036; the Guangdong Provincial Key Laboratory of Fishery Ecology and Environment under contract No. LFE-2015-3.
*Corresponding author, E-mail: liugm@nmefc.gov.cn

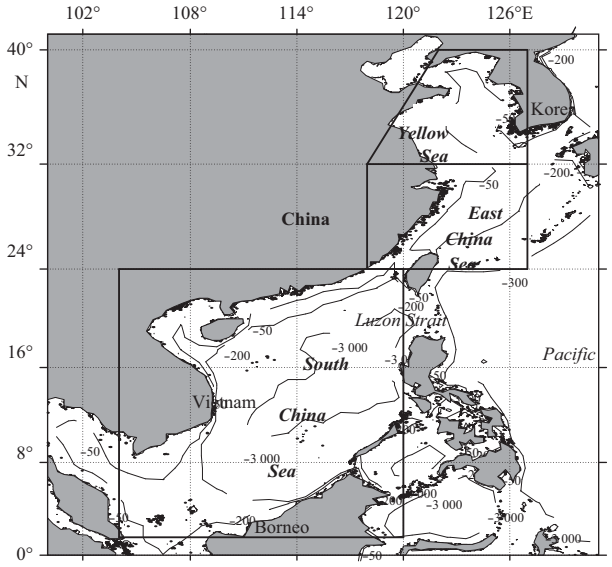

Fig. 1. Map of the China's seas.

from the Pacific Ocean by a chain of islands on the eastern side of the SCS, namely Borneo, Palawan and Luzon Islands.

The China's seas are in a position of special interest because they are geographically located between the Tibetan Plateau and western Pacific Warm Pool, two important regions that have great influences on global climate patterns. This interest has increased due to the urgent need to understand the relations between the carbon cycle and the global climate change. Dominated by the climate in the Tibetan Plateau and the western Pacific Warm Pool, the East Asia monsoon exhibits pronounced seasonal and inter-annual variations. The China's seas are influenced by the variability of the East Asia monsoon system. The most striking change is the seasonal variation of the East Asia monsoon: strong northeasterly monsoon prevails in winter, weak southwesterly monsoon in summer, and during the transition periods of spring and autumn, winds are weaker and more variable compared to the other two seasons. Due to the wind-stress curl and topography effect, there are strong seasonal variations in the circulations in the China's seas (e.g., Liao et al., 2005; Wu et al., 2005; Liao et al., 2006; Yuan et al., 2006). In addition, the Kuroshio influences the China's seas and drives the variability in those surroundings.

The spatial and temporal variations of carbon fluxes are controlled by diverse physical and biogeochemical processes in different regions in the China's seas (Nemoto et al., 2009; Tseng et al., 2009a, b; Hung et al., 2010). Physical processes, such as primarily sea surface warming/cooling, the mixing of surface waters and the ventilation of intermediate and deep waters are largely responsible for regulating the SST, therefore determining the air-sea CO_2 flux. On the other hand, the biological pump in many regions, the sinking of organic matter produced by phytoplankton and zooplankton, can have a stronger control on the oceanic pCO_2 than the physical process. Calculated from measured DIC and TA data in July 2007, Chou et al. (2009) thought that the Changjiang Diluted Water and Yellow Sea water areas were the two major sinks of atmospheric CO_2, the coastal upwelling area was the most important CO_2 source, and the Kuroshio water and Taiwan warm water areas were weaker sources. Nemoto et al. (2009) showed that the atmospheric pCO_2 had little variation (341–365 μatm) in the ECS, whereas oceanic pCO_2 in the surface water varied significantly (308–408 μatm) from June 29, 1997 to January 6, 1998. Using an underway system with continuous flow equilibration in January 2008, Chou et al. (2011) stated that the entire ECS shelf acted as a CO_2 sink in winter, with low oceanic pCO_2 in the warm and saline Kuroshio Current water and high oceanic pCO_2 in the cold and less saline Chinese coastal current water along the coast of China's mainland. Following the experiment that linked an equilibrator with a GC-102D gas chromatograph to determine the oceanic pCO_2 in the seawater designed by Cui et al. (2001), Ji et al. (2003) reported that the near-shore was the source of CO_2, the outer sea was the sink of CO_2, and the shelf area of the ECS was a net sink for atmospheric CO_2 in autumn 1994. In the SCS, the fugacity of CO_2 fluctuated between 340 and 400 μatm, closely following the temporal change in temperature and increasing at a rate of ~ 4 μatm/a with time (Chou et al., 2005; Tseng et al., 2007). In general, these previous studies were undertaken in a particular region with limited observational data. Further investigation on the carbon budget of the China sea system requires fully chemical and biogeochemical characterization.

Within this context, a Pacific basin-wide physical-biogeochemical model has been established to investigate the biological process and parameter optimization in the Chinese coastal seas (Ji et al., 2015). In particular, the main focus is toward diversity in temporal and spatial variations of primary production and oceanic pCO_2 among the SCS, the ECS, and the YS, and the controlling factors of oceanic pCO_2 are also examined by comparing the distribution of SST, chlorophyll *a* (Chl *a*), nutrients, primary production, and export flux in the SCS, the ECS, and the YS. Furthermore, the oceanic pCO_2 increase in the China's seas from 1982 to 2005 in response to the anthropogenic atmospheric pCO_2 increase are estimated.

2 Integrated physical and biogeochemistry carbon model

The physical model for this study is developed with the Regional Ocean Model System (ROMS), which represents an evolution in the family of terrain-following vertical-coordinate models. Ji et al. (2015, 2017) have configured the ROMS circulation model for the Northwestern Pacific Ocean (NWP, 3°–52°N, 98°–158°E) with 8-km horizontal resolution using realistic geometry and topography. There are 22 vertical sigma levels. The topography data is derived from GEBCO (General Bathymetric Chart of the Oceans) (https://www.bodc.ac.uk/data/online_delivery/gebco/), which is a global 30 arc-second grid largely generated by combining quality-controlled ship depth soundings with interpolation between sounding points guided by satellite-derived gravity data. Considering the influence of inflow and outflow at the boundary, we set the southern, eastern and northern boundaries as open boundary (Blumberg and Kantha, 1985). The lateral boundary conditions used for the physical model are FSCHAPMAN, M2FLATHER, M3RADIATION, M3NUDGING, TRADIATION and TNUDGING. Under the climatology run, the data for temperature, salt, zeta, u, v, ubar and vbar in the three open boundaries are derived from SODA (Simple Ocean Data Assimilation) climatological data (http://soda.tamu.edu/assim/SODA_2.2.4/). While during the high-forcing run, the lateral boundary data is from SODA monthly data. In the initial field, temperature and salinity are derived from the World Ocean Atlas (WOA2009) data in December with a spatial resolution of 1°×1° and 24 vertical layers (http://www.nodc.noaa.gov/OC5/WOA09/netcdf_data.html), while, u, v and zeta are set as zero.

The biogeochemical model is built upon the imbedded carbon and nitrogen ecosystem model developed by Fennel et al.

(2006). The NPZD model includes nitrate and ammonium, one phytoplankton group, one zooplankton grazer, two detritus pools, dissolved oxygen, total inorganic carbon and total alkalinity (Fig. 2). Considering the characteristics of marine ecosystems in the China's seas, the relevant biological process formulation in study area has been optimized and improved (Ji et al., 2015, 2017).

Before being coupled with the biogeochemical model, the circulation model based on ROMS is run for 20 years, and the results show that the circulation model could provide a more suitable physical condition to the biogeochemical model (Ji et al., 2017). Hence, after the circulation model reaches a steady state, the biogeochemical model is coupled into the circulation model with 8-km spatial resolution. The coupled modeled is run for 10 years under climatological conditions. After the initial ten-year spin-up, the basin-scale ROMS-NPZD model is forced with daily air-sea fluxes derived from the NCEP2 reanalysis from 1979 to 2005. The surface wind stress is calculated from the 10-m wind based on the Large and Pond (1982) drag coefficient formulation. The heat flux is obtained from the prescribed short- and long-wave radiations, sensible and latent heat fluxes are calculated following the bulk formula with prescribed air temperature and relative humidity. The fresh-water flux is obtained from the prescribed precipitation and the evaporation derived from the latent heat release.

As for the biological variables, the NO_3, total alkalinity (TA), total inorganic carbon (TIC) and dissolved oxygen (DO) are initialized from the WOA2009 in December. The Chl *a* in the initial field is derived from SeaWiFS (http://oceandata.sci.gsfc.nasa.gov.SeaWiFS) following a vertical interpolation formula (Morel and Berthon, 1989). For the phytoplankton and zooplankton, the initial fields are calculated from the phytoplankton/Chl *a* ratio of 0.5, and for the other four detritus, the initial fields are based on calculation of the detritus/phytoplankton ratio of 0.35 (Gruber et al., 2006). NH_4 is set as a constant value of 1 mmol/m^3 (calculated by nitrogen).

In the lateral boundary, the boundary fields of NO_3, TA, TIC and DO are from WOA2009. The boundary field of Chl *a* is calculated from monthly climatology data from SeaWiFS, and for the other variables the fields are calculated from Chl *a* using a correlation coefficient. The calculation function for the vertical Chl *a* concentration is following Morel and Berthon (1989), which is as follows:

$$Chl = Chlze \times \left(Chlb + Chl_{\max} \times \exp\left(-\left((zeta - zeta_{\max}) / \Delta zeta \right)^2 \right) \right), \quad (1)$$

where *Chlze* is the average concentration value of Chl *a* at the thickness of photiczone, $Chl_{\max}$ is the maximum value of Chl *a* concentration, *Chlb* is the surface concentration of Chl *a*, *zeta*=*Z*/*Ze*, *Z* is the seawater depth, and *Ze* is the thickness of photiczone.

River discharges, including Huanghe River (Yellow River), Changjiang River (Yangtze River), Zhujiang River (Pearl River) and Meikong River, are also set up with nutrient sources (NO_3 and NH_4) (Zhang, 1996; Duan and Zhang, 1999; Zhang et al., 2010).

3 Results and discussion

The evaluation of the NWP basin-scale ROMS–NPZD model has been conducted for the Chinese coastal seas (Ji et al., 2015, 2017). Ji et al. (2015, 2017) uses the same model output to compare the modeled temperature, salinity and biological variables with observations. Parameter sensitivity of the ecosystem also

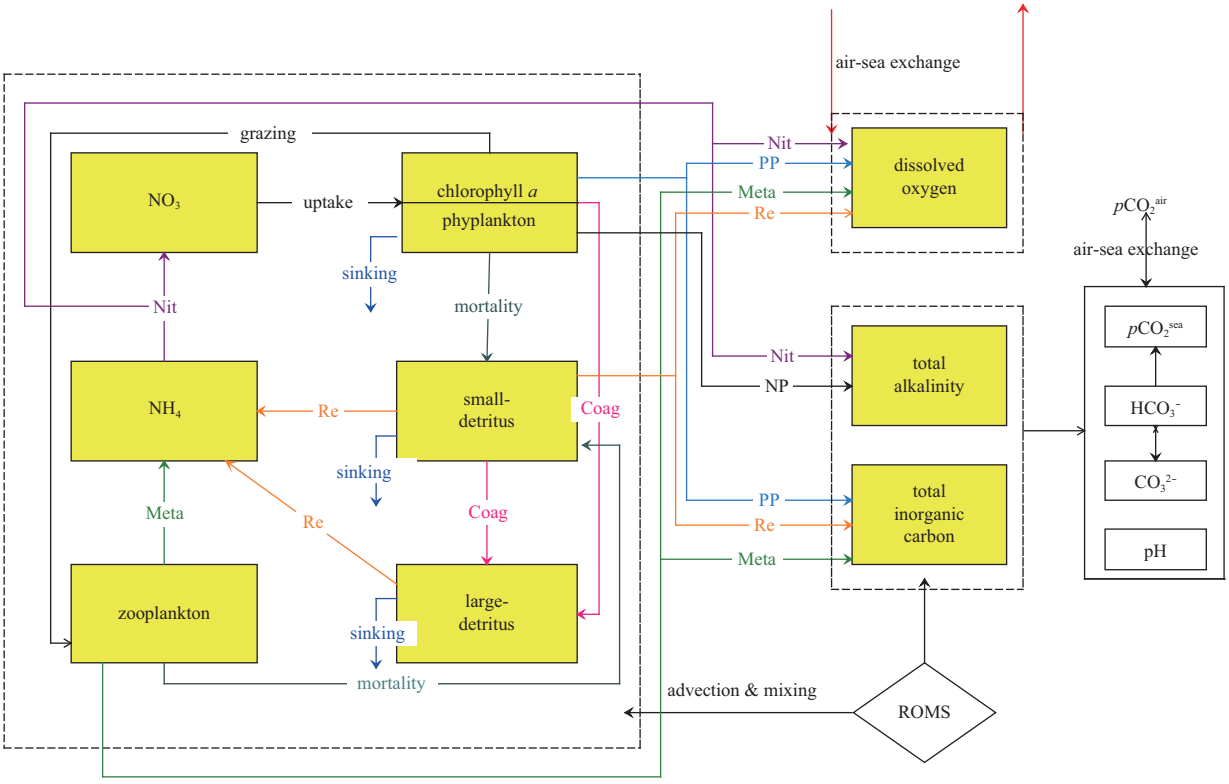

Fig. 2. A schematic of the nitrogen-based biogeochemical model. Nit represents nitrification, PP primary production, Meta metabolism, NP new production, and Re remineralization.

has been analyzed in the Chinese coastal seas (Ji et al., 2015). Therefore, as the first order comparison, the model successfully reproduces many observed features, which suggests that the model captures large scale and mean conditions of the key physical and biological processes in the NWP, including some of its marginal seas.

3.1 *Variability characteristics of pCO_2 in the three seas*

We average the monthly model output during the 1982–2005 period to produce the oceanic climatological pCO_2 spatial distributions in winter (January) and summer (July). In January (Fig. 3a), the surface water is mainly under-saturated and the oceanic climatological pCO_2 value ranges from 230 to 400 μatm in the study area. The oceanic pCO_2 increases from the northern YS to the southern SCS. The spatial variation of oceanic climatological pCO_2 is notable in sub-regions of the SCS, the ECS and the YS. In the YS (32°–40°N), the oceanic climatological pCO_2 is between 240 to 290 μatm, which is the lowest compared with those in the ECS and the SCS. The oceanic climatological pCO_2 value is between 270 and 360 μatm in the ECS (24°–32°N). Strongly correlated with the latitude, higher oceanic pCO_2 value appears in the south and lower value appears is in the north. In the SCS (5°–24°N), the oceanic climatological pCO_2 value is the highest, which ranges from 320 to 400 μatm. It is clear that the oceanic climatological pCO_2 is much lower than the atmospheric pCO_2 level in the YS and ECS, and thus these regions act as sinks to the atmospheric CO_2 in January. There are small areas in the southern SCS, where the oceanic pCO_2 level is higher than that in the air, but the SCS average oceanic climatological pCO_2 during winter is still lower than the pCO_2 level in the atmosphere, which indicates the entire SCS is a sink to the atmospheric CO_2 in January as well.

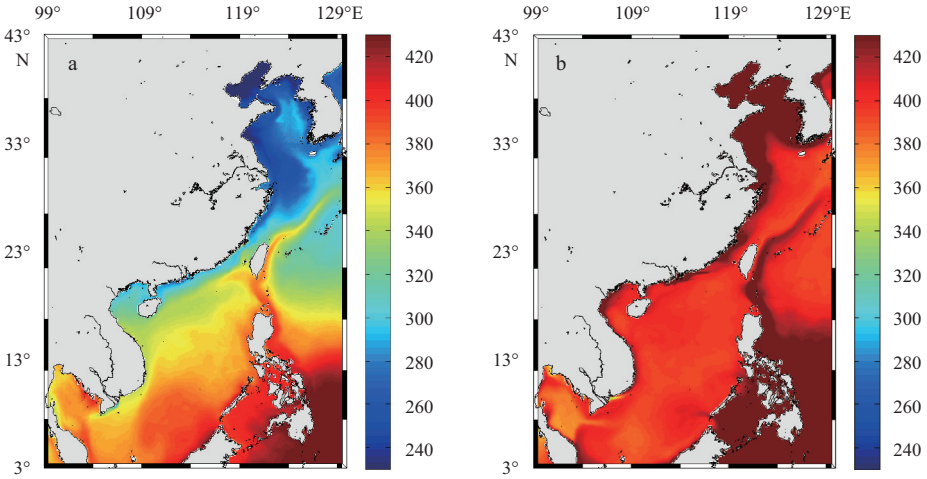

Fig. 3. Distribution of climatologic pCO_2 (μatm) in January (a) and July (b) during 1982–2005 in the China's seas.

In July, the maximum oceanic pCO_2 can reach 480 μatm, which is much higher than that in January (Fig. 3b). The oceanic pCO_2 value in the surface water is near saturation or is supersaturated compared to the atmospheric pCO_2 value. Unlike the great spatial discrepancy in the sub-regions in January, the oceanic climatological pCO_2 values in July in the SCS, the ECS, and the YS are in the same range (380–480 μatm) and show less spatial variability. Compared with the observation data from Zhai and Dai (2009), the modeled results in the outer Changjiang Estuary and the central southern YS are a bit higher. The deviation may be a result of two factors: one is the potentially incorrect inputs of Changjiang River using the published data of Changjiang River from Zhang (1996) and another is that the horizontal resolution of the model in the nearshore is insufficient to fully simulate the biological progress and carbon cycle.

3.2 *Seasonal cycle of the SST, Chl a, Nitrate and pCO_2 in the three seas*

To investigate the regional difference of the carbon cycle in the China's seas, it is important to clarify the seasonal evolutions of the SST, Chl *a*, nitrate, and pCO_2 in the SCS, the ECS, and the YS (Fig. 4). The SSTs in the SCS, the ECS, and the YS change seasonally from 5°C to 30°C (Fig. 4a). Except in the SCS, the SSTs in the ECS and the YS change seasonally in a sinusoidal pattern with a winter minimum and a summer maximum. The SCS average SST value shows obvious features of smaller seasonal amplitudes as well as stronger variability compared to the YS and the ECS. The monsoon transition periods in the SCS are believed to drive the seasonal variability of SST (Xie et al., 2003). Figure 4a shows that the water is the warmest in the SCS and the coolest in the YS. The extreme temperature difference in the three regions about 20°C, is found in winter with the lowest SST in the YS and highest SST in the southern part of the SCS. The temperature differences among the YS, the ECS, and the SCS are reduced to lowest in summer (Fig. 4a).

The average annual-mean surface Chl *a* is lower than 0.8 mg/m^3 (Fig. 4b), but shows great difference in the SCS, the ECS, and the YS. In the YS, the peak of Chl *a* occurs in March with a value of 0.7 mg/m^3. After the phytoplankton bloom in spring in the YS, the Chl *a* concentration stays at a low level, even less than 0.2 mg/m^3 in summer and autumn, and then begins to increase again. In the ECS, the Chl *a* concentration is lower than that in the YS in winter and early spring, but higher than that in the YS in later spring, summer and autumn. In the SCS, the Chl *a* concentration is less than 0.4 mg/m^3 during the annual cycle with two peaks: one in January and another in August, but the highest surface Chl *a* is in winter (Liu and Chai, 2009).

The average annual-mean surface nitrate concentrations are 1.89, 2.3, and 1.84 mmol/m^3 in the SCS, the ECS, and the YS (Fig. 4c). However, the seasonal variations of nitrate are large among these three regions. The highest nitrate concentrations in the three regions in winter are 3.5, 3.3, and 2.3 mmol/m^3 for the YS,

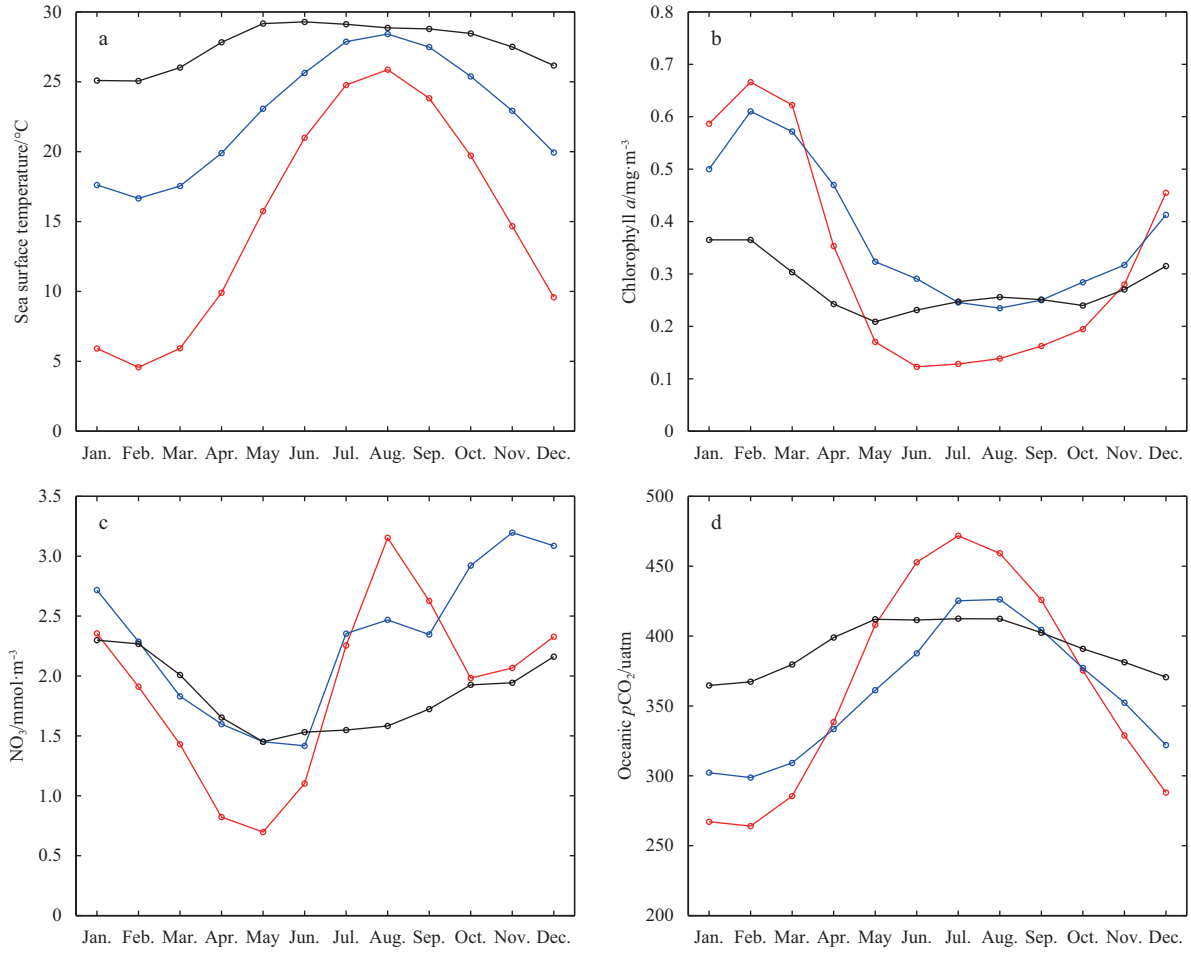

Fig. 4. Comparisons of multi-year averaged SST (a, °C), surface Chl *a* (b, mg/m^3), surface nitrate (c, mmol N/m^3) and oceanic pCO_2) (d, μatm) concentration in the Yellow Sea (red line), the East China Sea (blue line) and the South China Sea (black line).

ECS, and the SCS, respectively. The seasonal variations of SST, Chl *a*, and nitrate regulate primary productivity and carbon flux in the China's seas.

On a seasonal scale, the oceanic pCO_2 value, in the range of 260–480 μatm, is high in summer and low in winter in the SCS, the ECS, and the YS (Fig. 4d). The oceanic pCO_2 values indicate that the China's seas release CO_2 into the atmosphere only during summer, whereas CO_2 is transported to the ocean from the atmosphere in the other seasons. In August 1999, the pCO_2 was observed ranging from 300 to 500 μatm along the cruise line from Qingdao coast to the Jeju Island in the YS (Wang et al., 2002). In June and August 2003 in the ECS, it was observed that the pCO_2 was in the range of (301.6±61.0) μatm and (369.6±37.2) μatm, respectively (Chen et al., 2006). In October 1994, the pCO_2 was observed ranging from 310 to 390 μatm in the ECS, and the outer sea of the ECS was a sink of CO_2 (Ji et al., 2003). The modeled climatological results show reasonable agreement with the sparse observations in both the YS and the ECS.

The seasonal variability of oceanic pCO_2 is closely related to the seasonal warming/cooling of SST. Similar to the sensitivity study of pCO_2 to SST in the SCS (Chai et al., 2009), the temperature should also be an important controlling factor on the oceanic pCO_2 variation in the China's seas. However, the relationship of oceanic pCO_2 and SST varies among the YS, the ECS, and the SCS. During the winter, the oceanic pCO_2 is slightly higher in the SCS than those in the YS and the ECS. The northwesterly Asia monsoon prevails in winter in the YS and the ECS, which leads to vertical mixing in these seas. The vertical mixing induces low temperature, high productivity, and carbon-rich water from the bottom. Although the mixing brings water rich in CO_2 up from the bottom to the surface, low temperature (Fig. 4a) and high productivity in the mixing regions (Fig. 4b) seem to result in more draw-down of the CO_2.

3.3 *Seasonal cycle of biological productivity in the three seas*

The dominating physical processes in the SCS, the ECS, and the YS also drive regional diversity in biological productivity. To understand how the biological productivity and their regional differences affect the seasonal carbon cycle, we compare the climatological seasonal variations of primary production and new production in the three regions (Fig. 5 and Table 1). The climatological temporal evolutions of depth-integrated primary production (IPP), depth-integrated new production (INP), and the euphotic zone are presented at 50 m in the YS (0–50 m) and 75 m in the ECS (0–75 m) and the SCS (0–75 m).

The YS averaged climatological IPP ranges from 174 to 470 mg/(m^2·d) (calculated by carbon) with a strong seasonal feature (Fig. 5a). The peak of IPP in the YS is in April, at 490 mg/(m^2·d). The INP shows weaker variability, ranging from 92 to 202 mg/(m^2·d) (Fig. 5a). Based on satellite and *in situ* data, Zheng et al. (2006) calculated the integrated primary production in the YS, which is with the highest value in the spring (623 mg/(m^2·d)) and

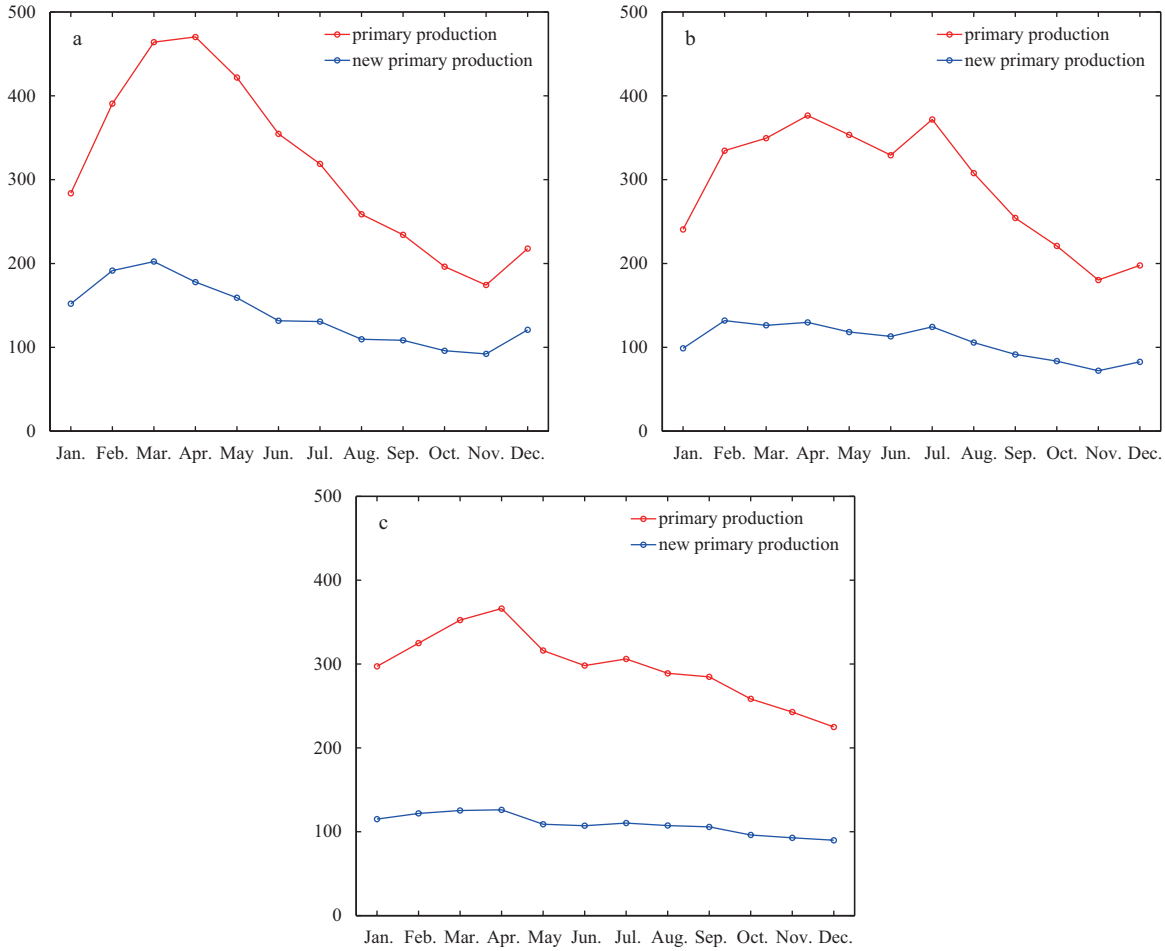

Fig. 5. The averaged climatologic seasonal succession of depth-integrated primary production (red line), new primary production (mg/(m^2·d)) (blue line) in the Yellow Sea (a), the East China Sea (b) and the South China Sea (c) respectively.

the lowest in winter (111 mg/(m^2·d)). The modeled results in this study agree with Zheng et al. (2006), but the peak value seems a bit smaller than the estimated results of Zheng et al. (2006). The coarse resolution (8 km) of the model might lead to the difference between the model and the observed integrated primary production, especially with many unresolved processes near the coast regions in the model. For example, processes such as the freshwater influences, water and sediment exchanges are not included in the model configuration. Such processes in coastal regions need to be incorporated for further basin-scale physical-biogeochemical modeling.

The ECS averaged climatological IPP varies from 190 to 390 mg/(m^2·d) (Fig. 5b). The IPP has double peaks: one in April with value of 375 mg/(m^2·d) and another in July with a value of 390 mg/(m^2·d). The lowest primary production appears in winter (from November to January), with a value range of 190–220 mg/(m^2·d). The modeled primary production is lower than the observation in the continental shelf region, which is less than 200 m in the ECS (Fig. 1). Gong et al. (2003) reported that the primary production was 515 mg/(m^2·d) in summer and 297 mg/(m^2·d) in winter. Apart from the lack of key processes in our model (like freshwater, water-sediment exchange), the difference between modeled and observed IPP in the ECS could also due to the different study areas for calculation, where the depth greater than 200 m was not included in Gong et al. (2003). The INP varies between 83 and 132 mg/(m^2·d) on a seasonal scale, and it is high in summer while low in winter over the entire ECS (Fig. 5b).

The SCS averaged IPP value falls between 230 and 390 mg/(m^2·d), with two peaks during a year (Fig. 5c). The first peak is in the winter from January to March, with a value of 390 mg/(m^2·d); another peak is smaller, which occurs in September with a value of 310 mg/(m^2·d). The lowest primary production show separately in June at 290 mg/(m^2·d) and in December at 250 mg/(m^2·d). The modeled seasonal evolution of IPP is consistent with the observations (Chen, 2005): the highest level of primary production is observed in winter, and the lowest is observed in summer; a slight increase is observed in fall. The modeled values of IPP fall in the range of observations, (500±260) mg/(m^2·d) in March and (370±170) mg/(m^2·d) in October (Chen, 2005). The difference between the modeled and observed may be due to the sampling limitation on spatial and temporal coverage. Liu et al. (2002) used a similar physical-biological modeling approach, and reported very similar seasonal variation of primary production in the SCS as ours. The INP in the euphotic zone varies from 90 to 126 mg/(m^2·d), which shows weaker variability than the primary production (Fig. 5c). The modeled new production seems to be lower than the existing limited observation data, (140±80) mg/(m^2·d) in March and (110±60) mg/(m^2·d) in October (Chen, 2005).

In addition to evaluate air-sea CO_2 flux, investigating the vertical carbon flux also improves our understanding of the total carbon budget. We estimate the vertical carbon export in terms of

f-ratio (new production/primary production), which theoretically should equal to the e-ratio (export production/primary production) under a steady state condition. During the period of 1982–2005, the total averaged annual-mean IPP and INP are 315 and 139 mg/(m²·d) in the YS (Table 1), respectively. Therefore, the averaged *f*-ratio is INP/IPP=0.45 in the YS. An *f*-ratio of 0.45 means that 45% of total carbon fixed exports vertically to the depth. In the ECS, the entire averaged IPP and INP are 297 and 109 mg/(m²·d), respectively. The averaged *f*-ratio is INP/IPP= 0.37, which is close to the *f*-ratio of 0.32 estimated by Chen and Chen (2003) using the field observations. The total averaged IPP and INP are 293 and 103 mg/(m²·d) in the SCS, respectively. So the *f*-ratio is INP/IPP=0.35, which is close to the value of 0.28±0.08, 0.32±0.14 observed in March and October of 2001 and 2002 in the northern part of the SCS (Chen, 2005). The lower *f*-ratio indicates low vertical carbon export in the SCS. The YS has the highest *f*-ratio comparing to the ECS and the SCS, which shows higher efficiency of transporting carbon out of the euphotic zone in the YS.

Table 1. Comparing annual mean carbon budgets in the Yellow Sea (32°–40°N, 118°–127°E), the East China Sea (24°–32°N, 118°–127°E) and the South China Sea (1.5°–24°N, 104°–120°E)

	Yellow Sea	East China Sea	South China Sea
IPP/mg·m^{-2}·d^{-1}	315	297	293
INP/mg·m^{-2}·d^{-1}	139	109	103
f-ratio	0.45	0.37	0.35
CO_2 flux/(mole C)·m^{-1}·a^{-1}	–1.05	–1.07	0.64
CO_2 flux/Tg·a^{-1}	–5.23	–6.73	16

3.4 *Sensitivity factors of controlling pCO_2 in the SCS, the ECS, and the YS*

Since SST and biological utilization regulate the air-sea carbon flux in the China's seas, it is necessary to separately investigate the effects of these two factors on controlling oceanic pCO_2 value. Generally, the effects of biological draw-down and SST on oceanic pCO_2 vary greatly according to regions. A series of sensitivity experiments were conducted by setting one factor as a constant with annual-mean value for SST, salinity, TIC, and total alkalinity, respectively, in order to isolate the effects. The standard experiment is based on the seasonal cycle of SST, salinity, TIC, and total alkalinity. Using the same estimated method given by Takahashi et al. (2002), the relative importance of the temperature effect on oceanic pCO_2 to the biological carbon utilization can be expressed as a ratio: $T/B=\Delta p_T CO_2/\Delta p_B CO_2$, where *T* refers to the temperature effect on the partial pressure of carbon dioxide in sea water, and *B* is the biological activity effect. Hence, the *T*/*B* ratios in the SCS, the ECS, and the YS are 1.22, 1.15, and 0.59 (Table 2), respectively, indicating that the SST effect is greater than the effect of biological activity on the carbon cycle in the SCS and ECS, and the temperature control is greater in the SCS than in the ECS. However, the effect of biological activity is greater than the SST effect on the carbon cycle in the YS. Therefore, the temperature control in the SCS and ECS is the primary driver dominating the oceanic pCO_2 change while the biological utilization plays a compensating role, and the biological activity control in the YS is the primary driver while the temperature is the second factor. This is quite similar when compared to the eutrophied coastal water and upwelling region, such as the southern bight of the North Sea in the Europe and the Changjiang River, where biological activity has a stronger influence on the seasonal oceanic pCO_2 cycle than the temperature (Zhai and Dai, 2009).

Table 2 shows the *T*/*B* ratios calculated by Takahashi et al. (2002): 2.7 at the Bermuda Atlantic Time-Series Study (BATS) in the North Atlantic (31°50′N, 64°10′W), 0.02 in the Ross Sea (76.5°S, 169–177°W), and 0.9 at the weather Station P in the North Pacific (50°N, 145°W). Using the global relative temperature and biology effects based on Takahashi et al. (2002), the biological effect is more obvious than the temperature effect in high latitude and upwelling region due to high primary production, and the temperature effect is stronger than biology effect in low latitude. Therefore, in the higher latitude of the Ross Sea, the biological effect is dominant and temperature effect is secondary. From this modeling study for the temperate regions, in the different regions, the effect of temperature and biological activity serve different roles in the China's seas.

Table 2. Temperature and biological productivity competing effects on the carbon cycle in the Yellow Sea (32°–40°N, 118°–127°E), the East China Sea (24°–32°N, 118°–127°E), the South China Sea (1.5°–24°N, 104°–120°E), Ross Sea of Antarctica (76.5°S, 169°E–177°W), Station P of North Pacific (50°N, 145°W), and BATS (31°50′N, 64°10′W)

Region	*T*/*B* ratio	Reference
Yellow Sea	0.59	this paper
East China Sea	1.15	this paper
South China Sea	1.22	this paper
Ross Sea of Antarctica	0.02	Takahashi et al. (2002)
Station P of North Pacific	0.9	Takahashi et al. (2002)
BATS	2.7	Takahashi et al. (2002)

3.5 *Variation trends of carbon fluxes and pCO_2 in the three seas*

For the air-sea CO_2 flux, there are long-term variation trends of the carbon fluxes in the SCS, the ECS, and the YS (Fig. 6). The air-sea CO_2 flux varies between the range of 8.51 and 6.34 mol/(m²·a) in the China's seas, with the lowest air-sea CO_2 flux in winter varies from year to year. The variability of air-sea CO_2 flux is more significant in the YS, followed by the ECS, then the SCS, which is likely resulted from the spatial and temporal differences. The SCS with lower primary productivity has the oligotrophic water, while the YS and the ECS have higher productivity. The biological pump is partially responsible for these regional discrepancies. On the annual-mean basis (averaged from the period of 1982–2005), the model results show that the YS and ECS are sinks for the atmospheric CO_2, while the SCS is a source (Table 1). The multi-year averaged flux of CO_2 integrated over the entire SCS is 16 Tg/a, which is released to the atmosphere. This is mainly because that the SCS is warmer and has lower biological productivity compared to the YS and the ECS (Chai et al., 2009). On the contrast, larger CO_2 fluxes (–5.23 Tg/a and –6.73 Tg/a, respectively) are absorbed by the YS and the ECS. Positive oceanic pCO_2 and SST relationships (Figs 4a and d) suggest the SST is an important control factor on the CO_2 flux in the China's seas, and the biological uptake during spring and summer in the YS and the ECS are also worth considering.

The time series of oceanic pCO_2 shows pronounced interannual variability and clearly upward trends from 1982 to 2005 in the YS, the ECS, and the SCS when taking seasonal variation out of consideration (Fig. 7). The anomalous oceanic pCO_2 ranges from –30 to 50 μatm. The linear regression shows positive slopes for the oceanic pCO_2 in the YS, the ECS, and the SCS with values of 0.079, 0.09, and 0.14, respectively. The rate of oceanic pCO_2 increase from 1982 to 2005 by 0.91 μatm/a (the YS), 1.04 μatm/a

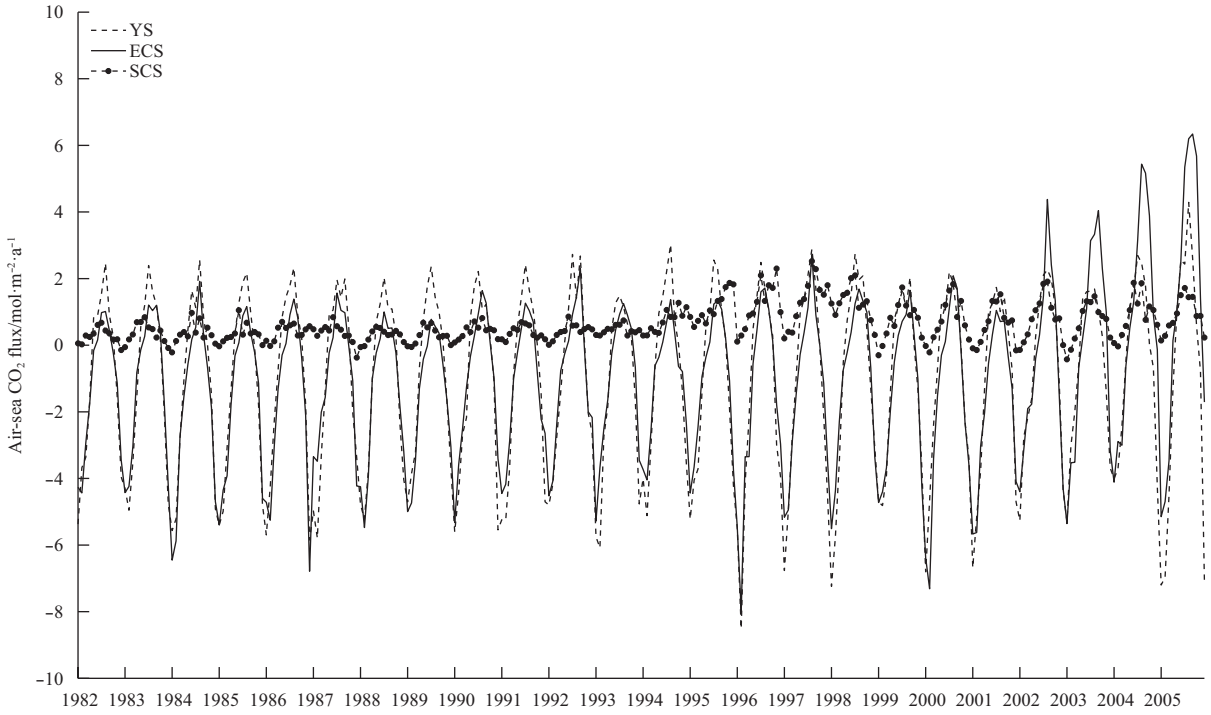

Fig. 6. Long-term variation trends of the monthly averaged air-sea CO_2 flux (mol/(m^2·a)) at the regions of the YS, the ECS and the SCS from 1982 to 2005.

(the ECS), and 1.66 μatm/a (the SCS), respectively. The reason for the modeled oceanic pCO_2 increase is due to the atmospheric pCO_2 goes up at a rate of 1.5 μatm/a on a global basis (Dore et al., 2003; Takahashi et al., 2003). The three regions are all positively affected by the atmospheric anthropogenic CO_2 increase, and the increase rate of oceanic pCO_2 is higher especially in the SCS. As shown in Fig. 7c, the anomalous oceanic pCO_2 in the SCS has a sudden change after 1995. Through analysis of several affecting variables, the dominant influence factor on oceanic pCO_2 is the increase of atmospheric pCO_2, and also the changes of physical and biological process were the secondary influence. The variable analysis will not be shown here in detail due to space limitations. According to the observed data at SEATS from 1999 to 2003, Tseng et al. (2007) estimated oceanic pCO_2 in the mixed layer increased at rates of (4.2±3.2) μatm/a. Hence, the modeled increasing rates of oceanic pCO_2 are in the range of their variability, and the small deviations may be a result of the calculated depth.

Recent studies confirmed the increasing trend of oceanic pCO_2 in the surface ocean. At the European Station for Time-series in the Ocean Canary Islands (ESTOC), oceanic pCO_2 increased at a rate of (0.71±5.1) μatm/a (Gonzalez-Davila et al., 2003). At the Station ALOHA near Hawaii (HOT), oceanic pCO_2 of seawater increased at a rate of (2.5±0.3) μatm/a (Dore et al., 2003; Keeling et al., 2004). At the BATS site in the Sargasso Sea between 1988 and 1998, oceanic pCO_2 increased at a rate of (1.4±5.1) μatm/a (Bates, 2001). Our model results show that the increasing rates of oceanic pCO_2 in the YS, the ECS, and the SCS are in line with the other long-term measures in the subtropical regions (ESTOC, HOT, and BATS), and highly agree with the atmospheric anthropogenic pCO_2 increase.

4 Conclusions

In this physical-biogeochemical modeling study, we used a Pacific basin-wide model to evaluate seasonal variation and long-term trend of oceanic pCO_2 in the SCS, the ECS, and the YS. The ROMS-NPZD simulations during the period of 1982–2005 show strong seasonal and inter-annual variations of primary production as well as the long-term increasing trend of oceanic pCO_2 due to increase of the atmospheric anthropogenic CO_2.

The ROMS-NPZD model simulations illustrate the complex interplay of physical and biological factors in determining variability of oceanic pCO_2 in the China's seas. The results suggest that the SST is a key factor that regulates spatial and temporal variations of the sea surface pCO_2. The biological removal of CO_2 plays a compensating role in modulating variation of the surface pCO_2, especially in the YS. During the period of 1982–2005, the modeled air-sea CO_2 fluxes in the China's seas alter from a sink in winter to a source in summer. On annual-mean basis, the SCS acts as a source of carbon to the atmosphere (16 Tg/a, released to the atmosphere), and the ECS and the YS are sinks to atmospheric CO_2 (–6.73 Tg/a and –5.23 Tg/a, respectively, absorbed by the ocean). The atmospheric pCO_2 increased from 1982 to 2005 due to the anthropogenic CO_2 input to the atmosphere. The oceanic pCO_2 increases in responses to the atmospheric pCO_2 that drives air-sea CO_2 flux in the model. The modeled increase rate of oceanic pCO_2 is 0.91 μatm/a in the YS, 1.04 μatm/a in the ECS, and 1.66 μatm/a in the SCS, respectively. The diversity of the model simulated primary and new productions among the SCS, the ECS, and the YS are linked to the seasonal variations of temperature and nutrients. The SST changed seasonally with a winter minimum value and a summer maximum value, while high nitrate concentrations appeared in winter and low concentrations were in summer in the China's seas. The SST in the SCS shows the smallest seasonal change compared to SST in the ECS and the YS, as well as the nitrate and Chl *a* change. The annual-mean IPP in the SCS, the ECS, and the YS is evaluated as 293, 297, and 315 mg/(m^2·d) by the present model simulation, which

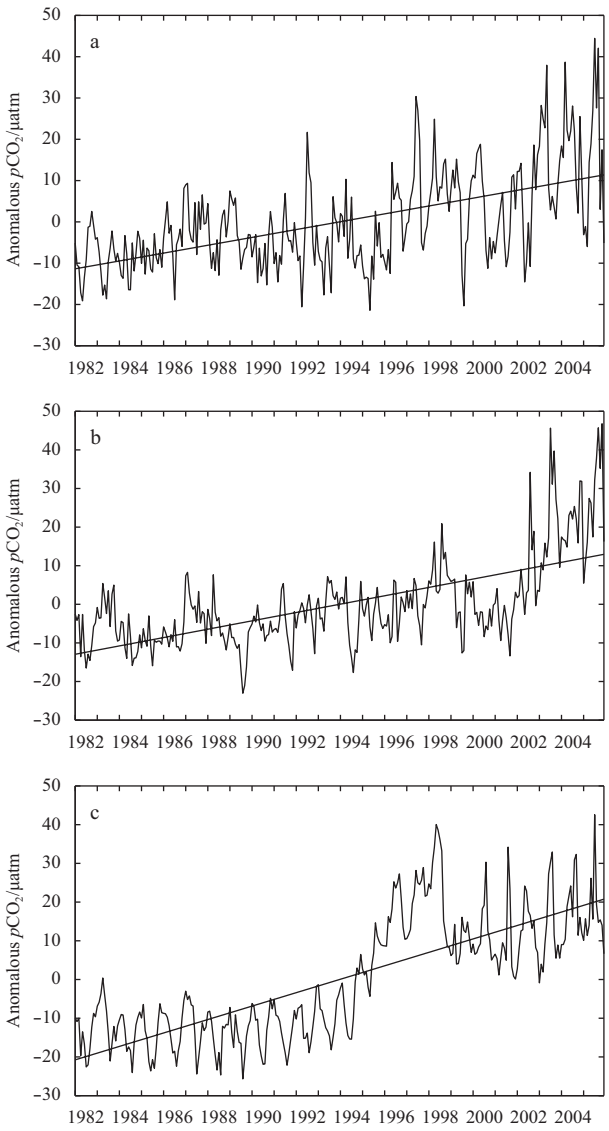

Fig. 7. Anomalous of oceanic pCO_2 in the YS (a: 0.079, 0.91 μatm/a), the ECS (b: 0.09, 1.04 μatm/a) and the SCS (c: 0.14, 1.66 μatm/a) from 1982 to 2005.

agrees fairly well with the recent estimates by field data. The model-integrated annual-mean new production is 103, 109 and 139 mg/(m^2·d), and yield the *f*-ratios of 0.35, 0.37 and 0.45 for the SCS, the ECS, and the YS, respectively. Compared to the productivity in the ECS and the YS, the seasonal variation of biological productivity in the SCS is the weakest. The estimation of primary productivity and carbonate system in the China's seas are a small glimpse of those that can be expected from environmental changes predicted in the near future in the context of global change and/or of management strategies. The model needs to be constrained and evaluated with more physical and biogeochemical observations, especially with simultaneous observations of biogeochemical variables and environmental factors. In future work, higher horizontal model resolution and more rivers are required to resolve the details of the vast shallow regions in the China's seas.

References

Bates N R. 2001. Interannual variability of oceanic CO_2 and biogeochemical properties in the Western North Atlantic subtropical gyre. Deep Sea Research Part II: Topical Studies in Oceanography, 48(8–9): 1507–1528, doi: 10.1016/S0967-0645(00)00151-X

Blumberg A F, Kantha L H. 1985. Open boundary condition for circulation models. Journal of Hydraulic Engineering, 111(2): 237–255

Cai Weijun, Dai Minhan, Wang Yongchen. 2006. Air-sea exchange of carbon dioxide in ocean margins: a province-based synthesis. Geophysical Research Letters, 33(12): L12603, doi: 10.1029/2006GL026219

Chai Fei, Liu Guimei, Xue Huijie, et al. 2009. Seasonal and interannual variability of carbon cycle in south China Sea: a three-dimensional physical-biogeochemical modeling study. Journal of Oceanography, 65(5): 703–720

Chen Y L L. 2005. Spatial and seasonal variations of nitrate-based new production and primary production in the South China Sea. Deep Sea Research Part I: Oceanographic Research Papers, 52(2): 319–340

Chen C T A, Andreev A, Kim K R, et al. 2004. Roles of continental shelves and marginal seas in the biogeochemical cycles of the North Pacific Ocean. Journal of Oceanography, 60(1): 17–44

Chen Y L L, Chen H Y. 2003. Nitrate-based new production and its relationship to primary production and chemical hydrography in spring and fall in the East China Sea. Deep Sea Research Part II: Topical Studies in Oceanography, 50(6–7): 1249–1264

Chen C C, Chiang K P, Gong G C, et al. 2006. Importance of planktonic community respiration on the carbon balance of the East China Sea in summer. Global Biogeochemical Cycles, 20(4): GB4001, doi: 10.1029/2005GB002647

Chou W C, Gong G C, Sheu D D, et al. 2009. Surface distributions of carbon chemistry parameters in the East China Sea in summer 2007. Journal of Geophysical Research, 114(C7): C07026, doi: 10.1029/2008JC005128

Chou W C, Gong G C, Tseng C M, et al. 2011. The carbonate system in the East China Sea in winter. Marine Chemistry, 123(1–4): 44–55

Chou W C, Sheu D D D, Chen C T A, et al. 2005. Seasonal variability of carbon chemistry at the SEATS site, northern South China Sea between 2002 and 2003. Terrestrial, Atmospheric and Oceanic Sciences, 16(2): 445–465

Cui He, Ji Lei, Wang Jun, et al. 2001. Method for *in situ* determination of pCO_2 in sea-air equilibrium system. Chinese Journal of Oceanology and Limnology, 19(2): 172–177

Dore J E, Lukas R, Sadler D W, et al. 2003. Climate-driven changes to the atmospheric CO_2 sink in the subtropical North Pacific Ocean. Nature, 424(6850): 754–757

Duan Shuiwang, Zhang Shen. 1999. The variations of nitrogen and phosphorus concentrations in the monitoring stations of the three major rivers in China. Scientia Geographica Sinica (in Chinese), 19(5): 411–416

Fennel K, Wilkin J, Levin J, et al. 2006. Nitrogen cycling in the middle Atlantic bight: results from a three-dimensional model and implications for the North Atlantic nitrogen budget. Global Biogeochemical Cycles, 20(3): GB3007, doi: 10.1029/2005GB002456

Fletcher S E M, Gruber N, Jacobson A R, et al. 2006. Inverse estimates of anthropogenic CO_2 uptake, transport, and storage by the ocean. Global Biogeochemical Cycles, 20(2): doi: 10.1029/2005GB002530

Gong G C, Wen Y H, Wang B W, et al. 2003. Seasonal variation of chlorophyll *a* concentration, primary production and environmental conditions in the subtropical East China Sea. Deep Sea Research Part II: Topical Studies in Oceanography, 50(6–7): 1219–1236

Gonzalez-Davila M, Santana-Casiano J M, Rueda M J, et al. 2003. Seasonal and interannual variability of sea-surface carbon dioxide species at the European Station for Time Series in the Ocean at the Canary Islands (ESTOC) between 1996 and 2000. Glob Biogeochem Cycles, 17(3): 85

Gruber N, Frenzel H, Doney S C, et al. 2006. Eddy-resolving simula-

tion of plankton ecosystem dynamics in the California current system. Deep Sea Research Part I: Oceanographic Research Papers, 53(9): 1483–1516

Hung C C, Gong G C, Chou W C, et al. 2010. The effect of typhoon on particulate organic carbon flux in the southern East China Sea. Biogeosciences, 7(10): 3007–3018

Ji Lei, Cui He, Xin Shuping, et al. 2003. Characters of the pCO_2 and CO_2 flux in the East China Sea in Autumn. Chinese Journal of Oceanology and Limnology, 21(2): 180–186

Ji Xuanliang, Liu Guimei, Gao Shan, et al. 2015. Parameter sensitivity study of the biogeochemical model in the China coastal seas. Acta Oceanologica Sinica, 34(12): 51–60

Ji Xuanliang, Liu Guimei, Gao Shan, et al. 2017. Temporal and spatial variability of the carbon cycle in the east of China's seas: a three-dimensional physical-biogeochemical modeling study. Acta Oceanologica Sinica, 36(3): 60–71

Keeling C D, Brix H, Gruber N. 2004. Seasonal and long-term dynamics of the upper ocean carbon cycle at Station ALOHA near Hawaii. Global Biogeochemical Cycles, 18(4): GB4006, doi: 10.1029/2004GB002227

Large W G, Pond S. 1982. Sensible and latent heat flux measurements over the ocean. Journal of Physical Oceanography, 12(5): 464–482

Liao Guanghong, Yuan Yaochu, Wang Zhanggui. 2006. The three dimensional structure of the circulation in the South China Sea during the summer of 1998. Haiyang Xuebao (in Chinese), 28(5): 15–25

Liao Guanghong, Yuan Yaochu, Xu Xiaohua. 2005. The three dimensional structure of the circulation in the South China Sea during the winter of 1998. Haiyang Xuebao (in Chinese), 27(2): 8–17

Liu Guimei, Chai Fei. 2009. Seasonal and interannual variability of primary and export production in the South China Sea: A three-dimensional physical-biogeochemical model study. ICES Journal of Marine Science, 66(2): 420–431, doi: 10.1093/icesjms/fsn219

Liu K K, Chao S Y, Shaw P T, et al. 2002. Monsoon-forced chlorophyll distribution and primary production in the South China Sea: observations and a numerical study. Deep Sea Research Part I: Oceanographic Research Papers, 49(8): 1387–1412

Morel A, Berthon J F. 1989. Surface pigments, algal biomass profiles, and potential production of the euphotic layer: relationships reinvestigated in view of remote-sensing applications. Limnology and Oceanography, 34(8): 1545–1562

Nemoto K, Midorikawa T, Wada A, et al. 2009. Continuous observations of atmospheric and oceanic CO_2 using a moored buoy in the East China Sea: variations during the passage of typhoons. Deep Sea Research Part II: Topical Studies in Oceanography, 56(8–10): 542–553

Takahashi T, Sutherland S C, Feely R A, et al. 2003. Decadal variation of the surface water PCO_2 in the western and central equatorial Pacific. Science, 302(5646): 852–856, doi: 10.1126/science.1088570

Takahashi T, Sutherland S C, Sweeney C, et al. 2002. Global sea-air CO_2 flux based on climatological surface ocean pCO_2, and seasonal biological and temperature effects. Deep Sea Research Part II: Topical Studies in Oceanography, 49(9–10): 1601–1622

Takahashi T, Sutherland S C, Wanninkhof R, et al. 2009. Climatological mean and decadal change in surface ocean pCO_2 and net sea-air CO_2 flux over the global oceans. Deep Sea Research Part II: Topical Studies in Oceanography, 56(8–10): 554–577, doi: 10.1016/j.dsr2.2008.12.009

Tseng C M, Gong G C, Wang L W, et al. 2009a. Anomalous biogeochemical conditions in the northern South China Sea during the El-Niño events between 1997 and 2003. Geophysical Research Letters, 36(14): L14611, doi: 10.1029/2009GL038252

Tseng C M, Liu K K, Wang L W, et al. 2009b. Anomalous hydrographic and biological conditions in the northern South China Sea during the 1997–1998 El Niño and comparisons with the Equatorial Pacific. Deep Sea Research Part I: Oceanographic Research Papers, 56(12): 2129–2143

Tseng C M, Wong G T F, Chou W C, et al. 2007. Temporal variations in the carbonate system in the upper layer at the SEATS station. Deep Sea Research Part II: Topical Studies in Oceanography, 54(14–15): 1448–1468

Walsh J J. 1991. Importance of continental margins in the marine biogeochemical cycling of carbon and nitrogen. Nature, 350(6313): 53–55

Wang Feng, Zhang Longjun, Zhang Jing. 2002. A preliminary study of pCO_2 in the surface water of the southern Yellow Sea in summer. Journal of Ocean University of Qingdao (in Chinese), 32(6): 1007–1011

Wu C R, Tang T Y, Lin S F. 2005. Intra-seasonal variation in the velocity field of the northeastern South China Sea. Continental Shelf Research, 25(17): 2075–2083

Xie Shangping, Xie Qiang, Wang Dongxiao, et al. 2003. Summer upwelling in the South China Sea and its role in regional climate variations. Journal of Geophysical Research, 108(C8): 3261, doi: 10.1029/2003JC001867

Yuan Yaochu, Liao Guanghong, Wang Zhanggui. 2006. A three dimensional diagnostic modeling study of the South China Sea circulation before onset of summer monsoon in 1998. Haiyang Xuebao (in Chinese), 28(5): 1–14

Zhai Weidong, Dai Minhan. 2009. On the seasonal variation of air-sea CO_2 fluxes in the outer Changjiang (Yangtze River) Estuary, East China Sea. Marine Chemistry, 117(1–4): 2–10

Zhang Jing. 1996. Nutrient elements in large Chinese estuaries. Continental Shelf Research, 16(8): 1023–1045

Zhang Xiaoxiao, Yao Qingzhen, Chen Hongtao, et al. 2010. Seasonal variation and fluxes of nutrients in the lower reaches of the Yellow River. Periodical of Ocean University of China (in Chinese), 40(7): 82–88

Zheng Guoxia, Song Jinming, Dai Jicui, et al. 2006. Distributions of chlorophyll-A and carbon fixed strength of phytoplankton in autumn of the southern Huanghai Sea waters. Acta Oceanologica Sinica, 25(3): 68–81